SUPPORTING INFORMATION

Interfacial Forces are Modified by the Growth of Surface Nanostructures

Chongzheng Na and Scot T. Martin

Total number of pages: 9

Number of Tables: 5

Number of Figures: 3

Table S1. Chemistry of Experimental Solution

No.	1	2	3	4	5	6	7	8
$NaNO_3$ added (mM)	0.99	0.999	0.9999	0.999	0.995	0.99	0.98	0.9
HNO_3 added (mM)	0.01	0.001	0.0001					
NaOH added (mM)				0.001	0.005	0.01	0.02	0.1
Calculated pH	5.0	6.0	6.8	8.0	8.7	9.0	9.3	10
Measured pH	4.97	6.05	6.5	7.09	7.94	8.59	9.06	9.73
Total Dissolved CO2 (mM)[†]	0.02	0	0.0003	0.006	0.02	0.001	0.004	0.007
PCO_2 (atm)[†]	7×10^{-4}	0	4×10^{-6}	9×10^{-7}	2×10^{-7}	5×10^{-6}	3×10^{-6}	4×10^{-7}

[†] The lowering of pH from its calculated value is presumably due to the dissolution of carbon dioxide in the solution. The most abundant species of dissolved CO_2 is bicarbonate in the range of our experimental pH. Bicarbonate concentration was calculated using Visual MINTEQ 2.51, a rewritten of USEPA MINTEQA2 4.0 in Visual Basic by Jon Petter Gustafsson at the Royal Institute of Technology, Sweden (http://www.lwr.kth.se/English/OurSoftware/vminteq).

Table S2. Analysis of Variance and Parameter Estimates for the Regression to Equation 4 in Figure 1a[†]

Source	Degree of Freedom	Sum of Squares[‡]	Mean Square	F Value	Probability > F[*]
Equation 4	1	8533	8533	197	0.000015
Residual Error	120	5205	43.375		
Total Error	121	13738			

Parameter	Degree of Freedom	Estimate	Standard Error	*t* Value	Probability > |*t*|[**]
A	1	44	11	4	0.00011
B	1	151	44	3.4	0.0001

[†] F-test and *t*-test follow standard procedures outlined in *Introduction to the Practice of Statistics* by Moore and McCabe, W. H. Freeman and Company, New York, 1998

[‡] $R^2 = 8533/13738 = 0.62$.

[*] A small probability indicates that the regression is robust.

[**] Small probabilities indicate that both parameters are significant.

Table S3. Piecewise Linear Regression of $f_{max}(MnO_x)$ and pH in Figure 3a[†]

Variable	Value							
pH	5.0	6.0	6.5	7.1	7.9	8.6	9.1	9.7
Reconstructed pH_1	5.0	6.0	6.5	6.5	6.5	6.5	6.5	6.5
Reconstructed pH_2	0	0	0	0.6	1.4	2.1	2.6	3.2
$f_{max}(MnO_x)$ (pN)	43	21	8	22	32	40	57	74

Source	Degree of Freedom	Sum of Squares[‡]	Mean Square	F Value	Probability > F[*]
Model[§]: $f_{max} = a pH_1 + b pH_2 + c$	2	3052	1526	58	0.0003
Residual Error	5	132	26.4		
Total Error	7	3184			

Parameter	Degree of Freedom	Estimate	Standard Error	*t* Value	Probability > |*t*|[**]
a	1	23.4	3.7	6.3	0.0007
b	1	18.9	1.6	11.8	< 0.0001
c	1	160	22.4	7.1	0.0004

[†] F-test and *t*-test follow standard procedures outlined in *Introduction to the Practice of Statistics* by Moore and McCabe, W. H. Freeman and Company, New York, 1998.

[‡] $R^2 = 3052/3184 = 0.96$ and adjusted $R^2 = 0.95$.

[*] A small probability indicates that the regression is robust.

[**] Small probabilities indicate that all three parameters are significant.

[§] Equation 6 is obtained by converting this model back to two linear models, one for pH < 6.5 and the other for pH ≥ 6.5, using estimated values of *a*, *b*, and *c*.

Table S4. *t*-Tests on the Linearity of $f_{max}(MnCO_3)$, $h(MnO_x)$, $z_{max}(MnO_x)$, and $z_{max}(MnCO_3)$ with pH[†]

Dependent Variable	Parameter	Total Degree of Freedom	Estimate	Standard Error	*t* Value	Probability > |*t*|[‡]
$f_{max}(MnCO_3)$	slope	6	0.34	0.54	0.63	0.55
	Intercept	6	3.0	4.1	0.73	0.49
$h(MnO_x)$	slope	6	0.042	0.043	0.98	0.36
	Intercept	6	2.5	0.3	8.3	0.00016
$z_{max}(MnO_x)$	slope	6	0.011	0.19	0.06	0.96
	Intercept	6	2.0	1.4	1.4	0.21
$z_{max}(MnCO_3)$	slope	6	0.026	0.041	0.63	0.55
	Intercept	6	0.23	0.31	0.74	0.49

[†] *t*-test follows standard procedures outlined in *Introduction to the Practice of Statistics* by Moore and McCabe, W. H. Freeman and Company, New York, 1998

[‡] Large probabilities for the estimation of slopes indicate that there are no linear relations.

Table S5. Estimate of Colloid Particle Size and Cell Speed to Overcome the Repulsion Barrier over Oxide Nanostructures at pH 9.5

Process	Expression	Estimate
Electrostatic repulsion of MnO_x to the tip of the probe	$E_e = \int_{z=3.77}^{\infty} f_e dz = 9.6Ae^{-\frac{3.77}{9.6}} + 4.8Be^{-\frac{3.77}{4.8}}$	$E_e = 6.2\times10^{-19}$ J
Spherical colloid settling under gravity	$E_c = \frac{1}{2} m_c v_c^{\,2} = E_e$ $m_c = \frac{4\pi}{3} r_c^{\,3} \rho_c$ $\rho_c = 3.17\times10^{3}$ kg/m^{3} † $v = 2178\left(\frac{d_c}{2}\right)^2 \left(\rho_c - \rho_{H_2O}\right)$ ‡	d_c = 13.6 μm
Swimming bacteria	$E_b = \frac{1}{2} m_b v_b^{\,2} = E_e$ $m_b = \frac{4\pi}{3} r_b^{\,3} \rho_{H_2O}$ $r_b = 10^{-6}$ m	v_b = 17 mm/s

† from CRC Handbook of Chemistry and Physics, 77th Ed.

‡ from Stokes' law (see Hiemenz and Rajagopalan, *Principles of Colloid and Surface Chemistry*, Marcel Dekker, Inc., New York, 1997 for detail).

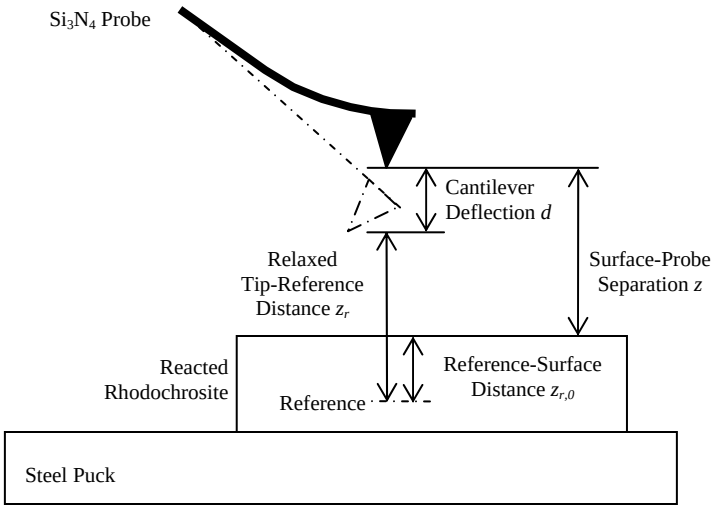

Figure S1. Experimental setup of force-curve measurement. The components above the steel puck are all immersed in solution. Drawing is not on scale. Cantilever deflection is greatly exaggerated. The force measurement is conducted as follows. The probe starts with its tip at a height of ca. 50 nm above the surface of reacted rhodochrosite and gradually approaches the surface in steps of less than 0.25 nm. At each step, the microscope records the distance, z_r, between the relaxed position of the probe tip (i.e., as if the tip did not experience any interfacial force and thus the probe cantilever did not bend) and a reference height. The reference height is established by a pre-run similar to the aforementioned approaching procedure so that when the relaxed position of the tip is at the reference height (i.e., $z_r = 0$), the tip is in contact with the sample surface under a preset force. The distance between the reference height and the surface is $z_{r,0}$, which can be readily determined on the resulting force curve. In addition to z_r, the microscope also records the vertical position of the tip by a laser beam shone on the back of the probe cantilever, which reflects the laser to a photodiode detector. The photodiode detector gives the vertical position in voltage V. By comparing with the voltage obtained when the tip is far away from the surface, V_0, voltage V gives the bending, commonly referred to as deflection, of the probe cantilever d. V, V_0, and d are related in a linear relation: $d = s(V - V_0)$ (S1-1) by detector sensitivity s. s is constant for each experimental setup with the same laser path length. The cantilever deflection responds to the interfacial force experienced by the probe tip. By convention $V - V_0$ and d are positive when the tip experiences a repulsive force. The actual distance between the tip and the surface (i.e., surface-probe separation) is: $z = z_r - z_{r,0} + d$ (S1-2). For a *rigid* surface such as rhodochrosite, whose deformation is negligible, Equation S1-2 is also valid when the tip is pressed in contact with the surface. Combining Equations S1-1 and S1-2 yields: $z_r = -sV + sV_0 + z_{r,0} + z$ (S1-3). Because $z = 0$ in the contact region and $sV_0 + z_{r,0}$ is constant, Equation S1-3 provides a convenient means to estimate s from a linear regression of V and z_r on the rhodochrosite substrate. Cantilever deflection d can be further converted to the interfacial force that the probe experiences using Hook's law: $f = kd$ (2), where k is the cantilever spring constant. Using the above equations, a force curve is converted from a V–z_r plot of the experimental data to a f–z plot that has a unambiguous physical meaning.

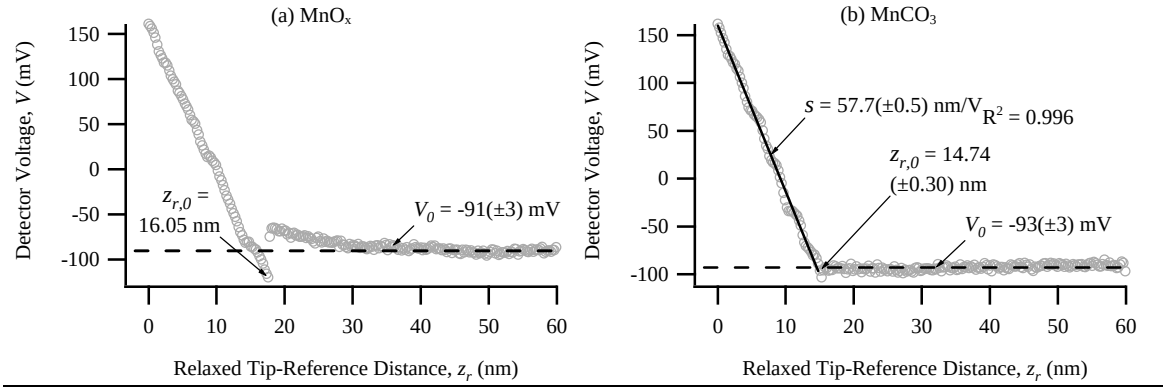

Figure S2. Raw data of the force curves shown in Figure 1. Detector sensitivity s is estimated from the force curves of the substrate and is used for the entire surface. Voltage reading when the sample surface and the SPM probe are far apart V_0 and relaxed tip-reference distance of the surface $z_{r,0}$ are obtained independently for rhodochrosite substrate and oxide nanostructures. The procedures used to estimate s, V_0, and $z_{r,0}$ are outlined as follows. For the typical V–z_r plot of rhodochrosite substrate as shown in Figure S2a, two regions can be identified—the contact region where the probe tip is pressed against the surface and the non-contact region where they are separate far apart. The contact region extends from z_r = 0 to ca. 15 nm where V increases proportionally to the decrease of z_r. The non-contact region spans from z_r = ca. 15 to 60 nm where V remains essentially constant. The intersect of these two regions gives $z_{r,0}(MnCO_3)$ = 14.74 nm. Detector sensitivity is estimated by performing linear regression to the data in contact region. The slope of the linearity gives s = 57.7(±0.5) nm/V. Averaging V over the non-contact region gives $V_0(MnCO_3)$ = -93(±3) mV. Similarly, contact and non-contact regions are also identifiable for the typical force curve of oxide nanostructures in Figure S2b. The contact region extends from z_r = 0 to ca. 17.5 nm where V increases monotonically with decreasing z_r whereas the non-contact region spans from z_r = ca. 17.5 to 60 nm with a complicated relation between V and z_r. The linearity of the contact region of oxide nanostructures, estimated to be 62.0(±0.4) nm/V, is however greater than the s value estimated using the contact region of the rhodochrosite force curve. Compared to the rigid rhodochrosite, this increased contact linearity indicates that deformation has occurred over oxide nanostructures when they are in contact with the probe tip. The deformation can be due to either the yield of surface materials under load or the high resistance in the last few layers of water molecules outside the surface (i.e., hydration force). We assign $z_{r,0}(MnO_x)$ = 16.05 nm so that the first point at the beginning of the contact region has z = 0 through Equation 2. The assignment agrees the physical constraint that measurement with a minimal load on the surface should have $z \equiv 0$. By doing so, we explicitly define the *surface* of oxide nanostructures to be at the point of $z_{r,0}(MnO_x)$ = 16.05 nm. The surface of oxide nanostructures can either locate at the actual interface between the nanostructures and the aqueous solution or at the interface between strongly bound water molecules and the weakly bound ones, depending on the mechanism of contact deformation. $V_0(MnO_x)$ = -91(±3) mV can be estimated at z_r > 40 nm where V becomes constant as the probe and the surface are separated far apart so that their interfacial force becomes negligible. We also use the s value estimated over the adjacent rhodochrosite substrate for the nanostructures because its value should be constant for a specific experimental setup.

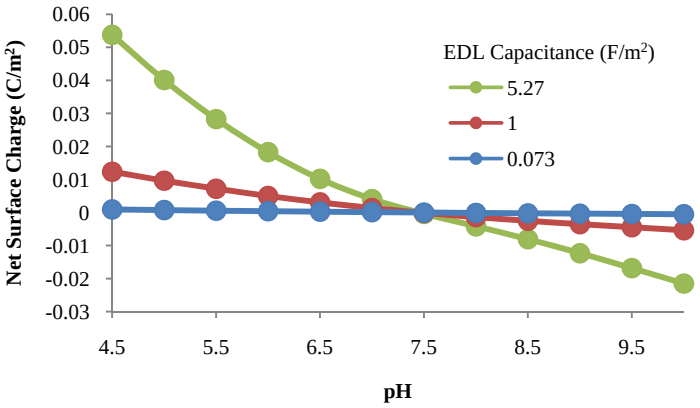

Figure S3. Estimation of rhodochrosite surface charge based on the surface complexation model. According to the model (van Cappellen et al., *Geochim. Cosmochim. Acta.* 57:3505-3518, 1993), the net surface charge of rhodochrosite is determined by six surface acid-base reactions: $>CO_3H^0 \Leftrightarrow >CO_3^- + H^+$ (S3-1), $>CO_3H^0 + Mn^{2+} \Leftrightarrow >CO_3Mn^+ + H^+$ (S3-2), $>MnOH^0 + H^+ \Leftrightarrow >MnOH_2^+$ (S3-3), $>MnOH^0 \Leftrightarrow MnO^- + H^+$ (S3-4), $>MnOH^0 + CO_2 \Leftrightarrow >MnHCO_3^0$ (S3-5), and $>MnOH^0 + CO_2 \Leftrightarrow >MnCO_3^- + H^+$ (S3-6). Under our experimental conditions where $[Mn^{2+}] < 10$ μM and $P_{CO2} < 0.0007$ atm, only Reactions (S3-1), (S3-3), and (S3-4) are significant. Van Cappellen et al. estimated the equilibrium constants of these reactions to be $K_1 = 10^{-5.0}$, $K_3 = 10^{-9.9}$, and $K_4 = 10^{-14}$. Because we conducted our experiments at pH 5.0 – 9.5 << pK_4, we can further neglect Reaction (S3-4). We further assume the total site density to be 9.2×10^{-6} mol/m^2, i.e., $[>CO_3H^0] + [>CO_3^-] = [MnOH^0] + [MnOH_2^+] = 9.2\times10^{-6}$ mol/m^2 (S3-7). Thus, the net surface charge is determined by the difference in concentration between oppositely charged surface species: $\sigma_{sub} = [MnOH_2^+] - [>CO_3^-]$ (S3-8). The equilibrium constants are further adjusted to surface potential ψ_{sub} to relate surface concentration to surface activity: $K_1^* = K_1\exp[-F\psi_{sub}/(RT)]$ (S3-9) and $K_3^* = K_3\exp[-F\psi_{sub}/(RT)]$ (S3-10), where F is Faraday's constant. Surface charge and potential can be related to each other by EDL models. Van Cappellen et al. used an empirical constant capacitance model $\psi_{sub} = \sigma_{sub}/C$ (S3-11), where C is the EDL capacitance and is determined by ionic strength I as depicted by $C(F/m^2) = I^{0.5}/0.006$ (S3-12). With I = 1 mM, C = 5.27 F/m^2. We realize that this value is much greater than the estimates of oxide surfaces that are usually around C < 1 F/m^2, which suggests the characteristics of the electrical double layer is different at the conditions of high ionic strength used by van Cappellen et al. from that under low ionic strength in our experiments. Under low ionic strength, the relation of ψ_{sub} and σ_{sub} is better approximated by the Graham equation (Stumm and Morgan, *Aquatic Chemistry*, John Wiley & Sons, 1996): $\psi_{sub} = \sigma_{sub}/(\varepsilon_0\varepsilon\kappa)$ (S3-11), where ε_0 is vacuum permittivity, ε is the dielectric constant of water, and κ is the reciprocal of the Debye length and equals $(9.6\text{ nm})^{-1}$ in 1 mM $NaNO_3$ solution at 25°C. The Graham equation gives $C = \varepsilon_0\varepsilon\kappa =$ 0.073 F/m^2. By trial and error, we solve Reactions (S1-1) and (S1-3) and Equations (S3-7) – (S3-11) simultaneously using C = 5.71, 1, and 0.073 F/m^2 at pH = 4.5 – 10 as shown in this figure. Apparently, the Graham equation that is applicable for low-potential conditions best describes our observation that the exposed rhodochrosite is essentially neutral from pH 5.0 to 9.5 in 1 mM $NaNO_3$ solution and in the absence of Mn^{2+} and dissolved CO_2.